Kovove Mater. 60 2022 13–20
DOI: 10.31577/km.2022.1.13

Fracture mechanism of mechanically alloyed Al composite

Oksana Velgosová[1]*, Štefan Nagy[2], Michal Besterci[3], Viktor Puchý[3], Zuzana Hájovská[2]

[1]*Institute of Materials and Quality Engineering, Faculty of Materials, Metallurgy and Recycling, Technical University of Košice, Letná 9, 042 00 Košice, Slovak Republic*
[2]*Institute of Materials and Machine Mechanics, Slovak Academy of Sciences, Dúbravská cesta 9/6319, 845 13 Bratislava, Slovak Republic*
[3]*Institute of Materials Research, Slovak Academy of Sciences, Watsonova 47, 040 01 Košice, Slovak Republic*

Received 9 December 2021, received in revised form 21 January 2022, accepted 17 February 2022

Abstract

In this study, the in situ tensile test in SEM was used for online observation of the deformation process and fracture mechanism of mechanically alloyed Al composite; also different techniques, including Scanning Electron Microscope (SEM), the Energy-Dispersive X-ray Spectroscopy (EDX), Transmission Electron Microscopy (TEM), Electron Diffraction and High-Resolution Scanning TEM (HR-S/TEM) were used for identifying of secondary phases. Microscopic analysis revealed spherical grains in the interval of 30–40 μm. The presence of intermetallic secondary precipitates Al-Fe-Si, Mg_5Si_6, and Al-Fe(Mn, Si) nanoparticles was confirmed. The in-situ test showed that the first cracks were created on the sample's surface and simultaneously in triple junctions of grains. Also, decohesion of Mg_5Si_6 and Al-Fe(Mn, Si) nanoparticles and rupture of large Al-Fe-Si particles were observed. Subsequently, the cracks propagated along the grain boundaries. The fracture surface is complex and composed of two systems. Based on the performed analysis, the model of fracture mechanism was proposed.

K e y w o r d s: mechanical alloying, Al composite, in-situ tensile test in SEM, fracture mechanism

1. Introduction

There is a growing need for advanced lightweight engineering materials that can provide the required strength, creep, tribology properties, high-temperature resistance, etc., at a reduced weight [1]. The researchers try to achieve the desired unique properties by a combination of different matrices (Al, Mg, …) and secondary phases (Al_2O_3, TiO, Y_2O_3, SiC, ThO_2, CNT, fullerenes, …) [2–4]. Due to the high tensile strength, low densities, and good corrosion resistance, dispersed light matrix composites are widely used in many applications, such as aircraft, automotive industry, sport, etc. [5, 6].

There are a lot of methods to fabricate dispersion strengthened Al composites as stir casting, high-energy ball milling, ultrasonic-assisted techniques, squeeze casting, friction stir welding, mechanical alloying, etc. The major problem and disadvantage of metal matrix composites are the relatively high costs of the process of fabrication. The cost-effective processing is, therefore, an essential element to produce composites. Among all, mechanical alloying (MA) is the promising and widely used method for preparing dispersion strengthened materials. MA method has a lot of advantages: achieving of fine structure, homogeneous distribution of dispersed phase, the process is performed at room temperature, MA process is also economically effective. Furthermore, the homogeneous distribution of particles results in good mechanical properties; such materials exhibit good plasticity, strength, creep properties, etc. [7–9]. Mechanical alloying (MA) has also been considered a viable method for the fabrication of nanocomposite materials [10].

The methods of preparation, mechanical properties, and the methods for improvement of dispersion strengthened composites characteristics were thoroughly researched and clarified; however, little attention was paid to the mechanism of fracture. The study of cracks initiation and analysis of the ways of

*Corresponding author: tel.: +421 55 602 2533; fax: +421 55 602 2770; e-mail address: oksana.velgosova@tuke.sk

their propagation is very important for determining the strength limits and fracture resistance of materials [11]. Such analysis also can help better understand the interfacial interactions and the influence of the morphology of the matrix grains and particles on fracture mechanism. Furthermore, the results of the fracture analysis can lead to improvement of the microstructure of the composite.

The in-situ tensile test in SEM is the best method for investigating fracture mechanisms because it enables observation and record of deformation processes directly. The initiation and development of the plastic deformation, initiation of cracks, and final fracture can be observed in real time and reliably described.

This work aimed to determine and characterize the structure elements (grain size, types of the secondary phases, their size, and shape) of mechanically alloyed IN-9052 Al alloy. Based on the in situ observation of the fracture mechanism, we also analyzed the behavior of these phases during the deformation process. The second aim was to study the damage initiation and failure of mechanically alloyed IN-9052 material, considering the impact of the matrix grains, particles' shape, size, and distribution. The in situ observation also allowed us to propose a simplified damage model of the mechanically alloyed IN-9052 Al composite system.

2. Materials and methods

The experimental material, NOVAMET IN-9052 alloy, is a commercial aluminum alloy produced by mechanical alloying. The nominal composition of the experimental alloy was: 4 Mg, 0.2 Fe, 0.5 Si, 1.1 Cu, 1.2 C, and 0.8 O in wt.%. The preparation of the alloy consisted of high-energy dry milling of aluminum alloyed with Mg and Cu and carbon in the form of carbon block in the presence of active grinding additives. Grinding particles were very small ($\sim 8\,\mu m$ in diameter), and iron contamination during grinding occurred. Grinding takes place in a protective atmosphere of argon. The obtained granules are degassed in a vacuum, then pressed by the hot isostatic pressing (HIP) method, and finally extruded. At room temperature, the alloy is characterized by a high yield strength of 620–650 MPa and a yield strength of 635–975 MPa, and a relatively high elongation of 10–14 %.

Electroerosive machining was used to prepare very small flat tensile test pieces (0.15 mm thickness). Next, the specimens were ground and polished down to the thickness of approximately 0.1 mm. Finally, the specimens were polished on both sides by ion beam milling with a PIPS instrument. The test pieces were fitted into the special deformation grips in the electron microscope JEOL SEM 5310, which enables direct observation of the deformation. Based on direct observation, both the deformation and failure processes (the crack initiation and propagation) of the test pieces were possible to detect. Qualitative analysis of secondary phases and matrix were realized by means of metallography, SEM (Jeol 6610), EDX (Oxford Instruments X-max 50 mm^2), TEM (Jeol 1200EX), electron diffraction, and HR-S/TEM (Titan Themis).

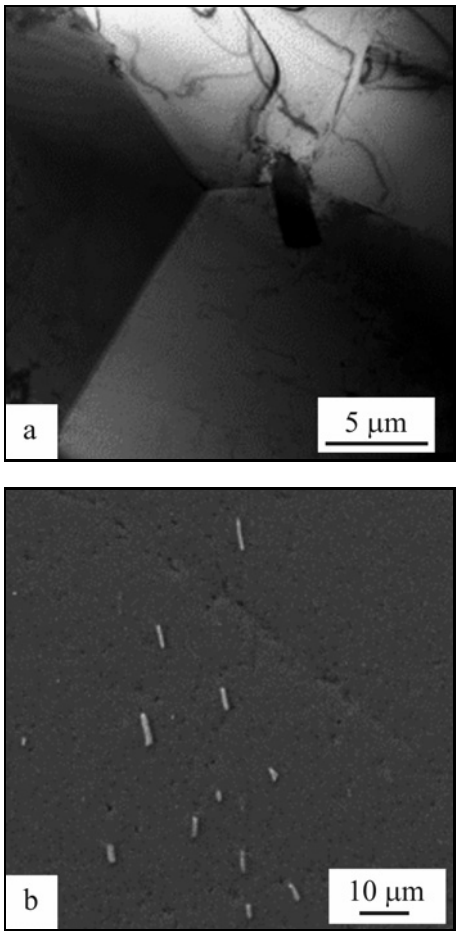

Fig. 1. TEM microstructure showing the matrix grain boundaries with an intermetallic Al-Fe-Si precipitate (a) and lower magnification SEM microphotograph of the sample microstructure with the same rod-like precipitates (b).

3. Results and discussion

3.1. Microstructure analysis

The results of the electron microscopy examination show that the composite has a polyhedral structure in which fine dispersion phases are located at the grain boundaries and inside the grains. The grains of the aluminum matrix are polygonal with a size in the interval of 30–40 μm. Figures 1a,b show the metallographically prepared microstructure and the grain boundaries of the sample with rod-like Al-Fe-Si parti-

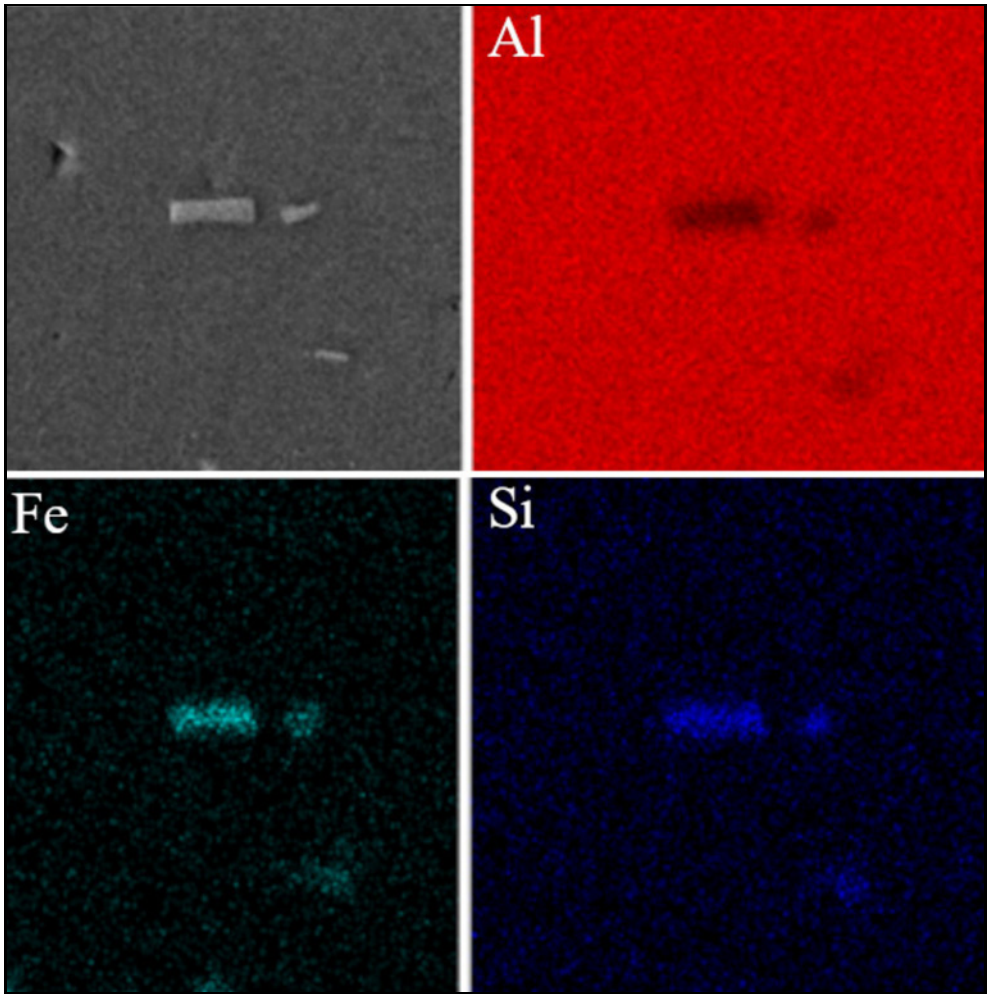

Fig. 2. SEM microphotograph of Al-Fe-Si (rod-like) particles and EDX map analysis.

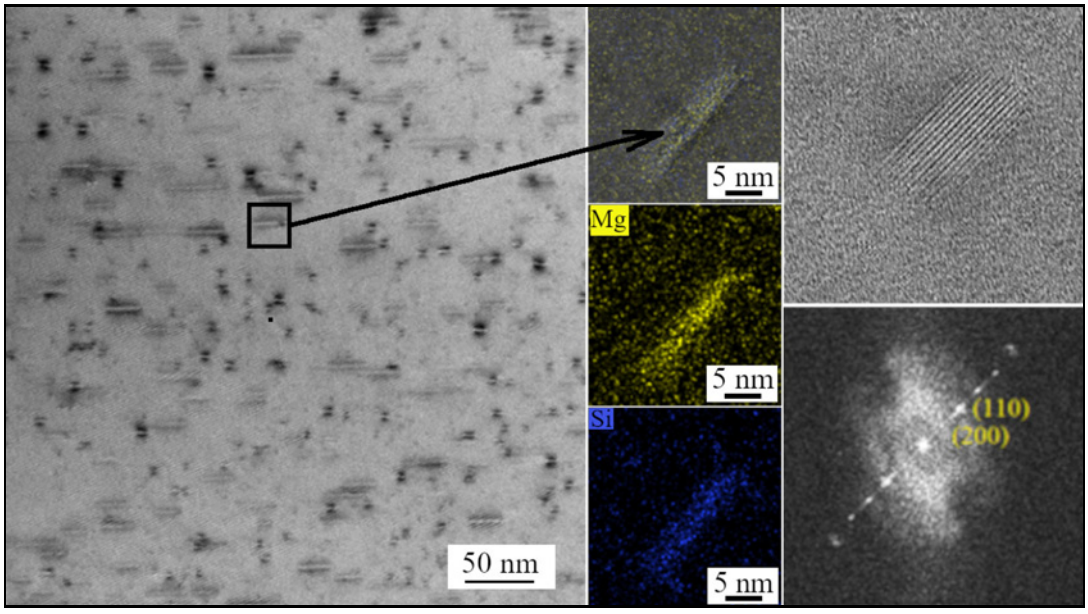

Fig. 3. STEM DF2 microphotograph, EDX analysis, and FFT diffraction of the Mg_5Si_6 (β'') phase.

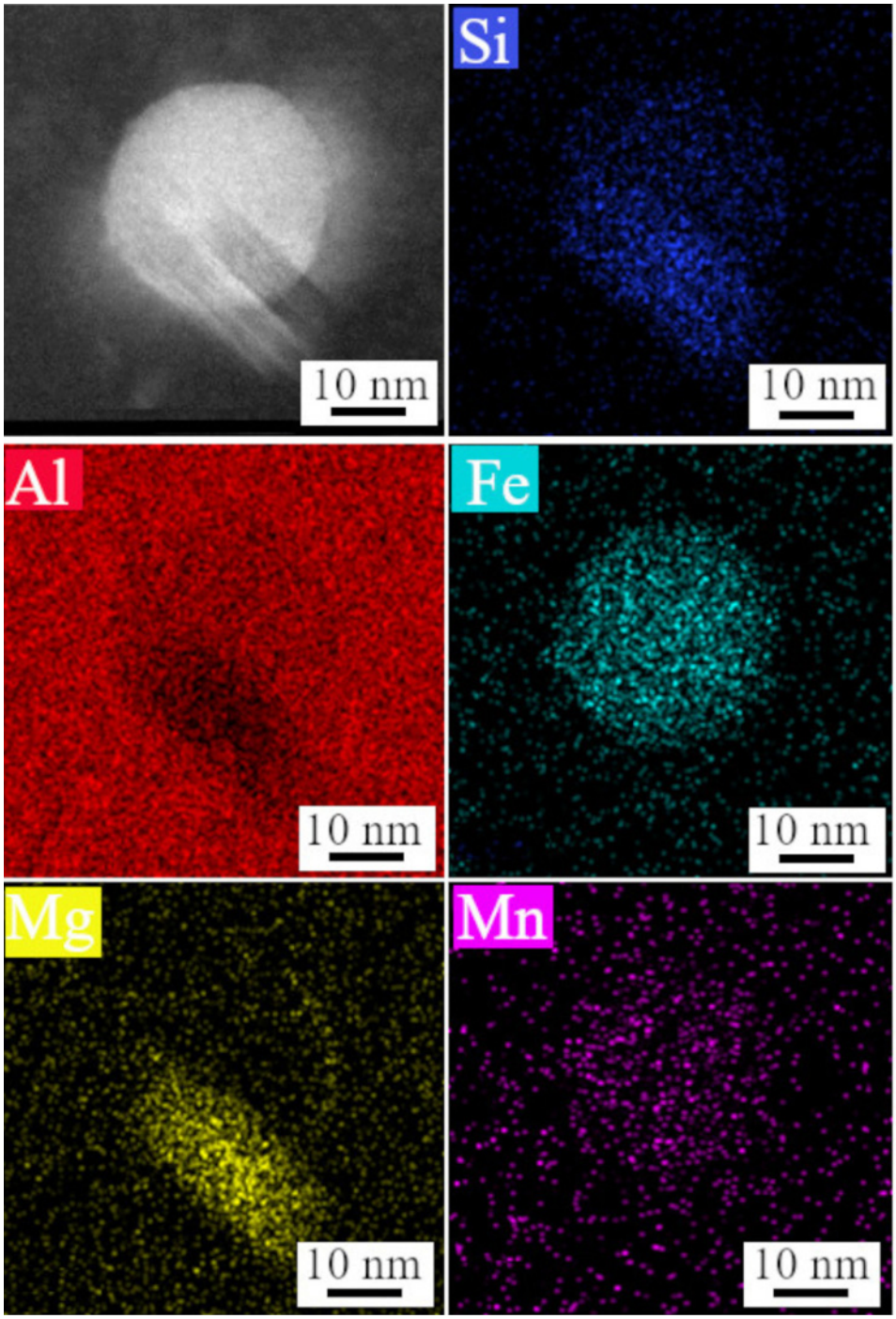

Fig. 4. STEM microphotograph and EDX analysis of Mg_5Si_6 needle-like and Al-Fe(Mn, Si) spherical nanoparticles.

cles confirmed with EDX analysis in Fig. 2.

Further investigation of the microstructure revealed precipitation on the nanometric level. For example, needle-like nano precipitates in Fig. 3 consisting of Mg and Si can be observed according to STEM and EDX analysis. In addition, the FFT diffractogram shows a good correlation of calculated crystallographic planes with the triclinic Mg_5Si_6 (β'') phase, which is an important hardening precipitate [12].

The next STEM micrograph and EDX map in Fig. 4 reveal Mg-Si precipitate and spherical precipitate containing primarily Al, Fe, and Mn elements, but Si is also measurable. The larger precipitates containing Fe and also the nano-precipitates can be classified into the iron-containing phases Al(Fe, Mn, Cr)Si. There can be different structures of these intermetallics that are associated with the morphology of Al-Fe-Si. The most common crystalline structures are

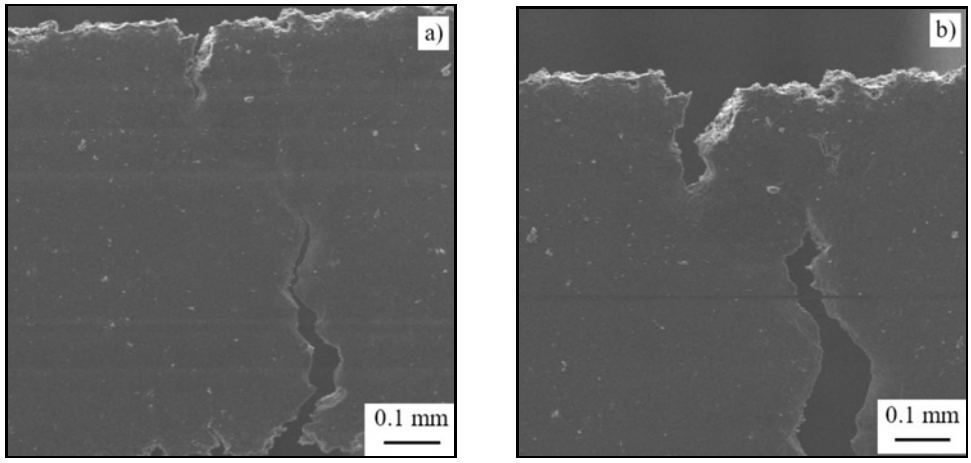

Fig. 5. Initiation (a) and propagation (b) of crack during specimen loading.

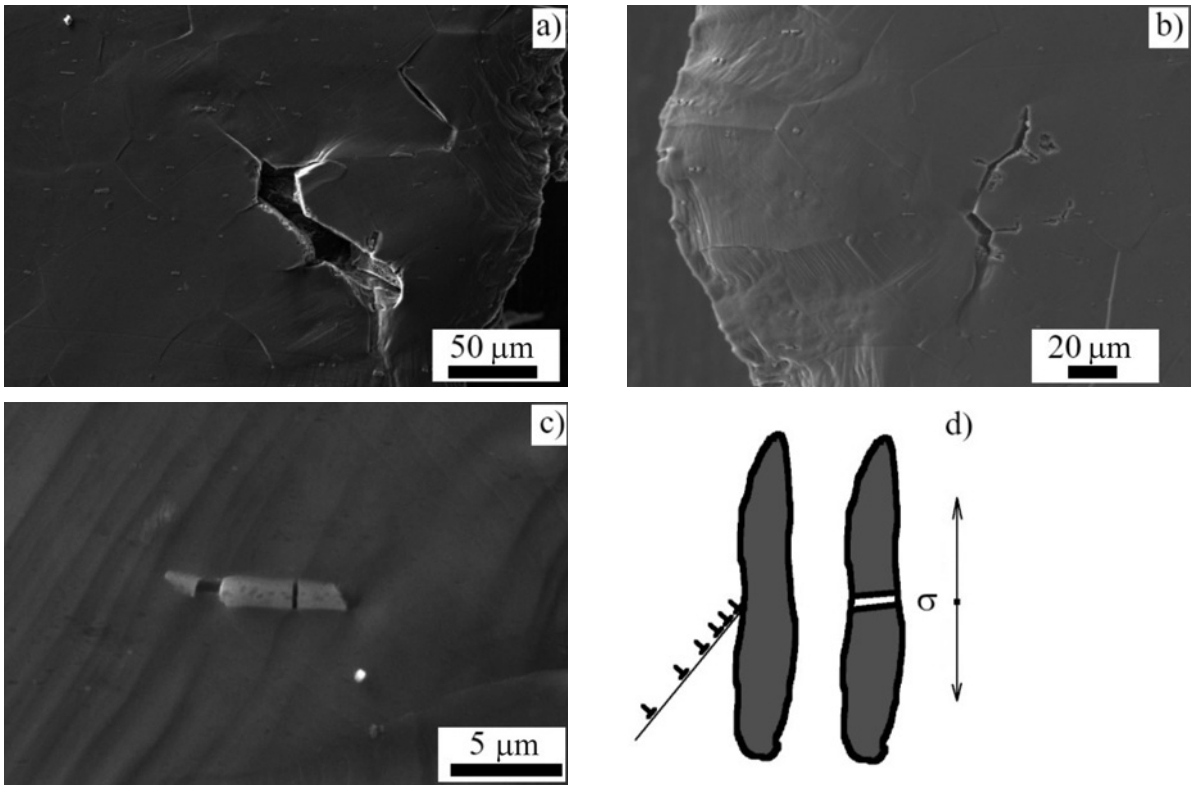

Fig. 6. Microfractures initiation in the triple grain junctions (a) and (b); cracking of secondary phase (c); the scheme of microdamage by secondary phase particle cracking (d).

monoclinic β-AlFeSi, cubic α-AlFeSi, and hexagonal α'-AlFeSi [13].

Intermetallic secondary precipitates can be separated into different categories:

– rod-like discontinuous large particles of Al-Fe-Si. Average size 5–7 µm and 1–2 µm in diameter.

– fine Mg_5Si_6 needle-like nanoparticles distributed quasi uniformly in a matrix with a size of about 5–40 nm (Fig. 3),

– Al-Fe(Mn, Si) spherical intermetallic nanoparticles with a mean size of about ~ 30 nm (Fig. 4).

3.2. Analysis of deformation and fracture mechanism

A tensile test was performed on the tensile test specimens at 20 ℃ at a deformation rate of $6.6 \times 10^{-4}\,s^{-1}$. With increasing stress, the first cracks were initiated on the surface and propagated approximately perpendicularly in the direction of the tensile load (Fig. 5).

During the deformation, the initiation of cracks was also observed in the triple grain junctions on the

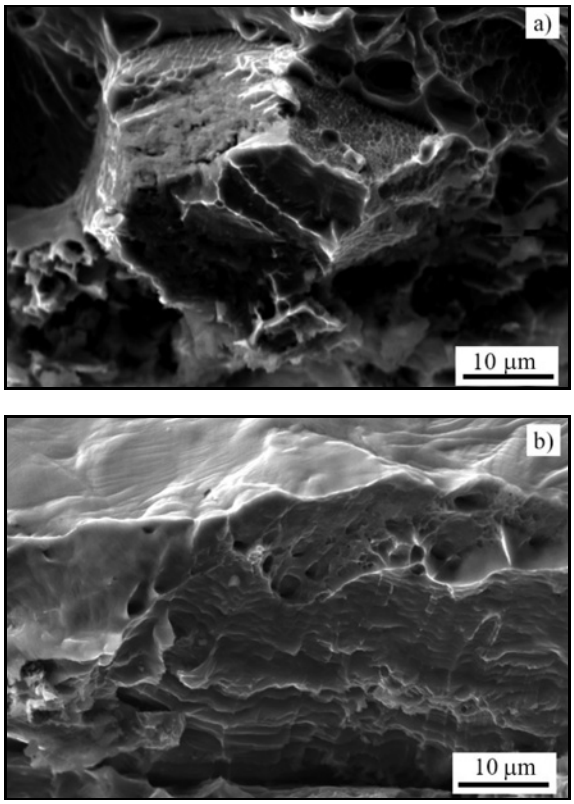

Fig. 7. Fracture surfaces with dimples and facets of intercrystalline fracture.

surface of tested samples [14]. With further loading, the cracks formed in triple points propagated along the grain boundaries (Figs. 6a,b), and the coalescence of cracks caused by triple grain junctions was observed. Also, under the influence of the applied stress, the plastic flow, and the accumulation of stress in the particles, cracks of large particles occured (Fig. 6c). The scheme in Fig. 6d corresponds to current notions about the nucleation of microdamage by secondary phase particle cracking.

The fracture surface of the tested sample is shown in Fig. 7. The micromechanism of failure of the analyzed system is very complex; the coexistence of the two systems on the fracture surface is obvious. There are facets of brittle intercrystalline fracture and the facets of ductile dimple fracture, Fig. 7. It can be concluded that ductile tearing, gradual ductile tearing, and shear tearing are applied within the ductile failure.

We assumed that in the case of a material with a plastic matrix and hard secondary phases, the material would damage by a ductile transcrystalline fracture with dimples. In this case, it was not so clear. Depending on the stress-strain processes, the formation, growth, and joining of cavities can lead to various dimple morphologies. If the growth and coalescence of the cavities take place in a zone where the plastic deformation takes place in several sliding systems, approximately uniform dimples or cavities are formed which are oriented in the direction of tensile stresses, and the dimples at the fracture surface are equiaxed. Such behavior is illustrated in the scheme in Fig. 8a. Unevenness in deformation processes in micro volumes of plastic materials often results in uneven development and uneven coalescence of the dimples. In this case, fracture propagation is gradually accompanied by local plastic deformation; the dimples are elongated in this case, shown by the scheme in Fig. 8b. If the failure occurs in the shear zone, then the failure is called a ductile shear rupture (Fig. 8c). These basic mechanisms of plastic failure have been experimentally confirmed in several systems.

A detailed study of the deformation changes showed that they were caused by decohesion of Mg-Si

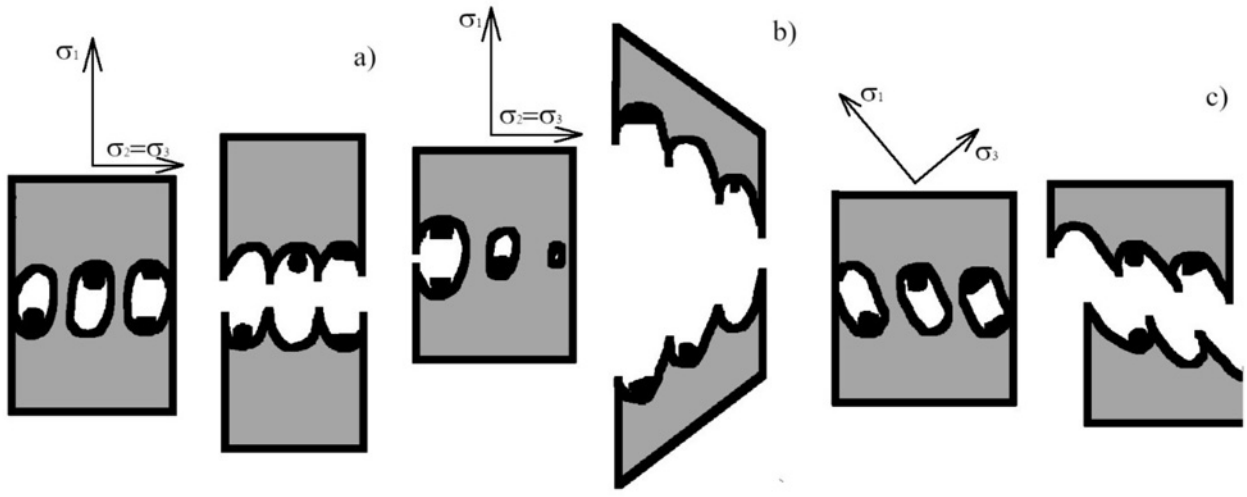

Fig. 8. Schemes of ductile fracture.

and Al-Fe(Mn, Si) particles, by rupture of large rod-like Al-Fe-Si, and by the formation of cracks in triple grain junctions.

Decohesion on the matrix-particles interface can result from different physical properties of phases presented in the system. The difference between the coefficients of thermal expansion of the particles and the matrix may create residual thermal stresses after cooling from the processing temperature to room temperature [15]. There is a significant difference between the Al matrix and, e.g., the Mg_5Si_6 phase. Matrix has higher thermal expansion coefficient and lower elastic modulus (α = 23.5–26.5 × $10^{-6}\,K^{-1}$, E = 70 GPa) than Mg_5Si_6 ($\alpha = 13.02 \times 10^{-6}\,K^{-1}$ and E = 110 GPa) [16]. Large differences in the thermal expansion coefficients result in high-stress gradients, which arise on the interphase boundaries during the hot extrusion. Since $\alpha_{matrix} > \alpha_{particle}$, high compressive stresses can be expected. However, because the stress gradients arise due to temperature changes, their partial relaxation can occur during cooling. Superposition of the external load and the internal stresses can initiate cracking at interphase boundaries. This is in accordance with the dislocation theories that argue that the particles in the composite may cause an increase in the dislocation density because of thermal strain mismatch between the ceramic particles and the matrix during preparation and/or thermal treatment. In our case, the coefficient of thermal expansion of the matrix is higher than that of the secondary particles, and the resulting thermal tension may relax around the matrix-particle interfaces by emitting dislocations.

Based on the analysis of initiation and propagation of the cracks observed during the in-situ deformation process, we proposed the model of fracture mechanism. The three steps of cracks initiation, propagation, and coalescence are shown in Fig. 9:

– The microstructure of the initial state: Al matrix and three categories of particles: A – rod-like large particles of Al-Fe-Si, B – fine Mg_5Si_6 needle-like nanoparticles, size of about 5–40 nm, and C – Al-Fe(Mn, Si) spherical nanoparticles with a mean size of about ∼ 30 nm.

– Increasing the tensile load caused the formation of the local cracks, predominantly on the surface of the sample (Figs. 5a, 6b), predominantly on the matrix-particles interface simultaneously, the cracks of particles category A occured (Fig. 6c).

– The further increase of the deformation caused propagation and coalescence of the cracks, preferentially along the grain boundaries (Fig. 6a).

4. Conclusions

The work aimed to characterize the structure, determine secondary phases in mechanically alloyed

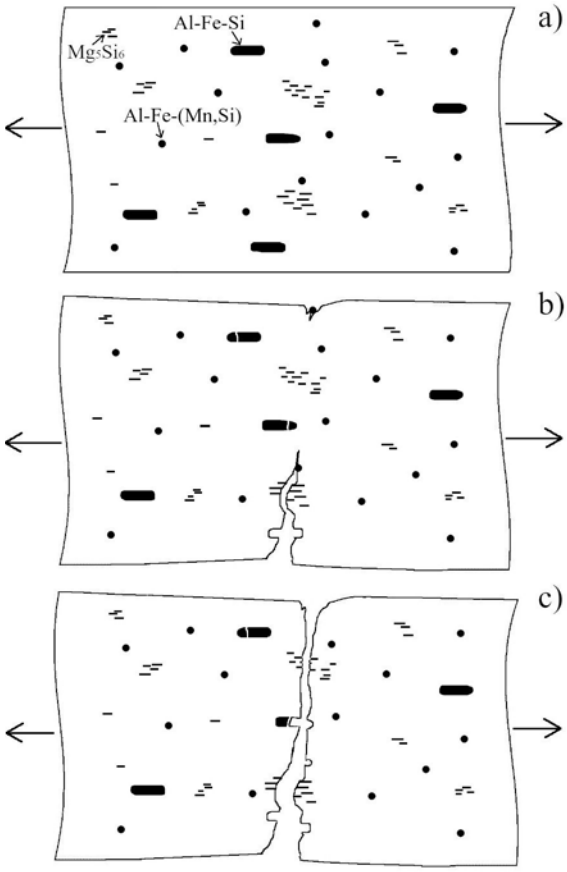

Fig. 9. The model of fracture mechanism.

IN-9052 Al alloy, and, based on the "in-situ" tensile test in SEM, observe and analyze the influence of microstructure components on the fracture mechanism. Based on the microscopical analysis, it was found that the aluminum matrix has a polyhedral structure with grains size 30–40 μm in diameter. Different types of fine dispersion phases were also determined: rod-like particles of Al-Fe-Si (average size 5–7 μm and 1–2 μm in diameter), fine Mg_5Si_6 needle-like nanoparticles with a size of about 5–40 nm, and Al-Fe(Mn, Si) spherical intermetallic nanoparticles with a mean size of about ∼ 30 nm. Dispersion phases were located at the grain boundaries and inside the grains.

The in situ tensile test in SEM observation of the deformation showed that the first cracks were initiated on the surface; also, the cracks were observed in the triple grain junctions. It was also observed that the increase of tensile load contributed to the fracture by the decohesion of Mg_5Si_6 and Al-Fe(Mn, Si) and by the rupture of large rod-like Al-Fe-Si particles. The SEM analysis of the failure surface showed that the failure micromechanism of the analyzed system is complex and is composed of two systems: the facets of brittle intercrystalline fracture and the facets of ductile dimple fracture. Also, a simplified model of the fracture mechanism was proposed.

Acknowledgement

The work was supported by the Slovak National Grant Agency under Project VEGA 2/0101/20.

References

[1] R. S. Rana, R. Purohit, S. Das, Review of recent studies in Al matrix composites, Int. J. Sci. Eng. Res. 3 (2012) 1–16.

[2] G. Garcés, M. Rodríguez, P. Pérez, P. Adeva, High temperature mechanical properties of Mg-Y_2O_3 composite: Competition between texture and reinforcement contributions, Compos. Sci. Technol. 67 (2007) 632–637. doi:10.1016/j.compscitech.2006.07.021

[3] L. Liu, K. Maeda, T. Onda, Z.-C. Chen, Effect of YSZ with different Y_2O_3 contents on toughening behavior of Al_2O_3/Ba-β-Al_2O_3/ZrO_2 composites, Ceramics International 45 (2019) 18037–18043. doi:10.1016/j.ceramint.2019.06.023

[4] Y. Xu, L. Cheng, L. Zhang, X. Luo, W. Zhou, Preparation and mechanical properties of self-reinforced in situ Si_3N_4 composite with La_2O_3 and Y_2O_3 additives, Composites: Part A 30 (1999) 945–950. doi:10.1016/S1359-835X(99)00013-5

[5] E. Tekoğlu, D. Ağaoğulları, S. Mertdinç, M. L. Öveçoğlu, Effects of reinforcement content and sequential milling on the microstructural and mechanical properties of TiB_2 particulate-reinforced eutectic Al-12.6 wt.% Si composites, J. Mater. Sci. 53 (2018) 2537–2552. doi:10.1007/s10853-017-1687-0

[6] P. Garg, A. Jamwal, D. Kumar, K. K. Sadasivuni, C. M. Hussain, P. Gupta, Advance research progresses in aluminium matrix composites: manufacturing & applications, J. Mater. Res. Technol. 8 (2019) 4924–4939. doi:10.1016/j.jmrt.2019.06.028

[7] C. Suryanarayana, N. Al-Aqeeli, Mechanically alloyed nanocomposites, Progress in Materials Science 58 (2013) 383–502. doi:10.1016/j.pmatsci.2012.10.001

[8] A. Orlová, K. Kuchařová, J. Čadek, Interpretation of creep in two aluminium alloys strengthened by nonshearable particles in terms of Estrin's constitutive model, Scripta Metallurgica et Materialia 29 (1993) 627–632. doi:10.1016/0956-716X(93)90408-K

[9] A. Orlová, J. Čadek, On Rösler and Arzt's new model of creep in dispersion strengthened alloys, Acta Metallurgica et Materialia 40 (1992) 1865–1871. doi:10.1016/0956-7151(92)90173-C

[10] A. Heidarpour, F. Karimzadeh, M. H. Enayati, Fabrication and characterisation of bulk Al_2O_3/Mo nanocomposite by mechanical milling and sintering, Powder Metall. 54 (2011) 513–517. doi:10.1179/003258910X12740974839585

[11] L. Mishnaevsky Jr., K. Derrien, D. Baptiste, Effect of microstructure of particle reinforced composites on the damage evolution: Probabilistic and numerical analysis, Comp. Sci. Technol. 64 (2004) 1805–1818. doi:10.1016/j.compscitech.2004.01.013

[12] S. J. Andersen, C. D. Marioara, J. Friis, S. Wenner, R. Holmesta, Precipitates in aluminium alloys, Advances in Physics: X 3 (2018) 1479984. doi:10.1080/23746149.2018.1479984

[13] A. Wimmer, J. Lee, P. Schumacher, Phase Selection in 6082 Al-Mg-Si Alloys, BHM Berg- und Hüttenmännische Monatshefte, 157 (2012) 301–305. doi:10.1007/s00501-012-0034-7

[14] M. Besterci, K. Sulleiová, T. Kvačkaj, Fracture micromechanisms of Cu nanomaterials prepared by ECAP, Kovove Mater. 46 (2008) 309–311.

[15] P. Lukáč, Z. Trojanová, Deformation and damping behaviours of microcrystalline Mg reinforced with ceramic nanoparticles, Kovove Mater. 44 (2006) 243–249.

[16] M. Imai, Y. Isoda, H. Udono, Thermal expansion of semiconducting silicide β-$FeSi_2$ and Mg_2Si, Intermetallics 67 (2015) 75–80. doi:10.1016/j.intermet.2015.07.015